SOILS AND FOUNDATIONS Vol. 46, No. 1, 99–108, Feb. 2006
Japanese Geotechnical Society

FEM SIMULATION OF THE VISCOUS EFFECTS ON THE STRESS-STRAIN BEHAVIOUR OF SAND IN PLANE STRAIN COMPRESSION

MOHAMMED S. A. SIDDIQUEE[i], FUMIO TATSUOKA[ii] and TADATSUGU TANAKA[iii]

ABSTRACT

A stress-strain model called TESRA (Temporary Effects of Strain Rate and Acceleration), described in a non-linear three-component framework, has been proposed to simulate the effects of viscous property on the stress-strain behaviour observed in drained plane strain compression (PSC) tests on clean sands. According to the TESRA model, the current viscous stress component is obtained by integrating for a given history of irreversible strain increments of viscous stress component that developed by respective instantaneous irrecoverable strain increment and its rate and have decayed with an increase in the irreversible strain until the present. The TESRA model was implemented into a generalized elasto-plastic isotropic strain-hardening non-linear FE code. The integration scheme to obtain the viscous and inviscid stress components according to the TESRA model in FEM analysis needs some specific considerations including the relevant choice of the suitable rate parameter. The shear stress—shear (or axial) strain—time relations from five drained PSC tests on saturated Toyoura sand and air-dried Hostun sand were successfully simulated by the FE code embedded with the TESRA model. It is shown that the FE code can simulate the time-dependent stress-strain behaviour of sand accurately without spending any significant extra computational time or storage. The results of simulation using one element and multi-element are essentially the same.

Key words: creep deformation, FEM simulation, loading rate effect, plane strain compression tests, sand, viscous property (**IGC**: D6/D7)

INTRODUCTION

The loading rate effects due to material viscosity on the stress-strain behaviour of sand (not due to delayed dissipation of excess pore water) are often very important in geotechnical engineering practice. A number of researchers (e.g., Di Benedetto and Tatsuoka, 1997; Lade and Liu, 1998; Matsushita et al., 1999; Di Benedetto et al., 2002; Tatsuoka et al., 2002; Kuwano and Jardine, 2002; Nawir et al., 2003a, b; Tatsuoka, 2004) reported significant loading rate effects observed in laboratory stress-strain tests on drained sand; i.e., effects of strain rate and its change on the stress-strain relation, creep deformation and stress-relaxation during otherwise monotonic loading (ML) at a constant strain rate.

Within the framework of the general non-linear three-component model (Fig. 1), Di Benedetto et al. (2002) and Tatsuoka et al. (2002) proposed a set of stress-strain models to simulate the effects of material viscosity on the stress-strain behaviour of geomaterial (i.e., clay, sand, gravel and sedimentary softrock). They showed that the viscous property of clean sand (i.e., uniform sand) is different from that of clay in that the viscous effect decays with an increase in the irreversible strain and proposed a specific model as described below.

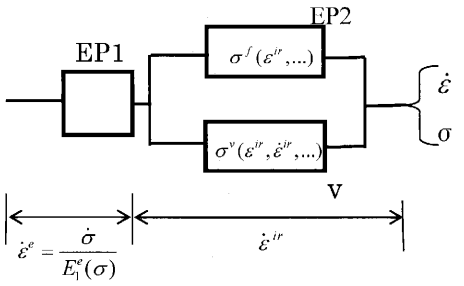

Fig. 1. Non-linear three-component model (Di Benedetto, 1987)

In this paper, it is shown that this model can be smoothly implemented in a FE code. Then, the shear stress—shear (or axial) strain relations obtained from typical drained plane strain compression (PSC) tests performed at fixed confining pressure on clean sands (i.e., Toyoura and Hostun sands), reported by Di Benedetto et al. (2002) and Tatsuoka et al. (2002), are simulated by the FE code embedded with the TESRA model.

[i] Civil Engineering Department, Bangladesh University of Engineering & Technology, Bangladesh.
[ii] Tokyo University of Science, Japan (tatsuoka@rs.noda.tus.ac.jp).
[iii] University of Tokyo, Japan.
The manuscript for this paper was received for review on August 30, 2004; approved on November 10, 2005.
Written discussions on this paper should be submitted before September 1, 2006 to the Japanese Geotechnical Society, 4-38-2, Sengoku, Bunkyo-ku, Tokyo 112-0011, Japan. Upon request the closing date may be extended one month.

MODEL DESCRIPTION

The non-linear three component model, depicted in Fig. 1, has the following general features:

1) A given total strain rate, $\dot{\varepsilon}$, is decomposed into the elastic component, $\dot{\varepsilon}^{e}$, and the irreversible (or inelastic or visco-plastic) component, $\dot{\varepsilon}^{ir}$ (or $\dot{\varepsilon}^{vp}$). Di Benedetto et al. (2002) assumed that $\dot{\varepsilon}^{e}$ takes place only in component *EP1*, while component *EP2* exhibits $\dot{\varepsilon}^{ir}$ only. This assumption greatly simplifies the model parameter determination. ε^{e} is obtained by integrating for a given stress path as $\varepsilon^{e}=\int d\varepsilon^{e}$, where $d\varepsilon^{e}=d\sigma/E^{e}(\sigma)$; where $E^{e}(\sigma)$ is the tangent elastic stiffness, which is a function of instantaneous stress σ (and others) (i.e., the hypo-(quasi)-elastic model; Tatsuoka and Kohata, 1995; Hoque and Tatsuoka, 1998; Tatsuoka et al., 1999).
2) The total component of a given effective stress, σ, which is herein called the total stress component, is decomposed into the time-independent (inviscid) and time-dependent (viscous) components, σ^{f} and σ^{v}, as:

$$\sigma=\sigma^{f}(\varepsilon^{ir}, h_{s})+\sigma^{v} \tag{1a}$$

where $\sigma^{f}(\varepsilon^{ir}, h_{s})$ means the σ^{f}-ε^{ir} relation, called the reference stress-strain relation, whatever strain (or stress) rates take place when traveling along a given strain (ε^{ir}) or stress (σ^{f}) path (with or without cyclic loading); and h_{s} is the parameter representing the loading history. Different σ^{f}-ε^{ir} relations are therefore formed for loading, unloading, reloading, cyclic loading and so on. Empirical σ^{f}-ε^{ir} relations obtained for the respective monotonic loading (ML) test to be simulated were used in the present study. Here, ML is defined as the loading condition where the irreversible strain rate, $\dot{\varepsilon}^{ir}$, is always positive whether its magnitude changes arbitrarily with time. σ^{v} is the viscous stress component, which is a function of ε^{ir} and its rate, $\dot{\varepsilon}^{ir}=\partial\varepsilon^{ir}/\partial t$, and the history parameter.

For primary ML along a fixed stress path, in which the irreversible strain rate, $\dot{\varepsilon}^{ir}$, is always positive, the history parameter h_{s} for σ^{f} in Eq. (1a) becomes unnecessary and Eq. (1a) is rewritten as:

$$\sigma=\sigma^{f}(\varepsilon^{ir})+\sigma^{v} \tag{1b}$$

In Eqs. (1a) and (1b), the stresses in the integral form are used, because they represent the stress summation, which cannot be represented in terms of stress increments. Moreover, the viscous stress component, σ^{v}, therefore, the total stress component, σ, is loading history-dependent cannot be properly described only in terms of stress increments. On the other hand, the general elasto-plastic model framework should be described incremental in the sense that total strain increments (elastic and plastic) can be defined in the objective way along with stress increments. It is also the case with the general elasto-viscoplastic model framework. In the present study, the solution algorithm of Eqs. (1a) and (1b) are formulated in an incremental way (Eqs. (9) and (10) in this paper) to be suitable for the FEM solution technique.

Moreover, the stresses, σ and the others, in Eq. (1) and other similar equations basically mean the stress tensors. A specific form of the respective stress tensor under general three-dimensional (3D) stress conditions are not known yet. In this paper, a one-dimensional form (with a single independent stress parameter) is first presented. Then, all the components of stress and strain tensors that are used in FEM analysis are formulated and expressed for plane strain conditions. Equations (11) and (12) (shown later in this paper) are an adaptation of the TESRA model in this specific case. By the use of yield surface and plastic potential function, the one-dimensionally expressed elasto-viscoplastic model can be extended to the general 3D stress space. Although one yield locus is used for the analysis under plane strain conditions in the present study, it can be extended to a multi-yield locus variant in a rather straightforward manner.

Di Benedetto et al. (2002) and Tatsuoka et al. (2002) showed that at least three different functional forms of the viscous component, σ^{v}, are necessary to describe the different viscous properties of geomaterial. Firstly, a stress-strain model called the "new isotach" was proposed to describe the loading rate effects of clay-like materials, for which, for primary ML along a fixed stress path, the current value of σ^{v} is a non-linear function of instantaneous value of $\dot{\varepsilon}^{ir}$ while it is always proportional to the instantaneous value of σ^{f} as:

$$\sigma^{v}(\varepsilon^{ir}, \dot{\varepsilon}^{ir})=\sigma^{f}(\varepsilon^{ir})\cdot g_{v}(\dot{\varepsilon}^{ir}) \tag{2}$$

$$\sigma=\sigma^{f}(\varepsilon^{ir})\cdot\{1+g_{v}(\dot{\varepsilon}^{ir})\} \tag{3}$$

where $g_{v}(\dot{\varepsilon}^{ir})$ is the viscosity function, which is always zero or positive and given as follows for any strain (ε^{ir}) or stress (σ^{f}) history (with or without cyclic loading):

$$g_{v}(\dot{\varepsilon}^{ir})=\alpha\cdot\left[1-\exp\left\{1-\left(\frac{|\dot{\varepsilon}^{ir}|}{\dot{\varepsilon}^{ir}_{r}}+1\right)^{m}\right\}\right] \quad (\geq 0) \tag{4}$$

where $|\dot{\varepsilon}^{ir}|$ is the absolute value of $\dot{\varepsilon}^{ir}$; and α, $\dot{\varepsilon}^{ir}_{r}$ and m are positive material constants. According to this model, as far as ML continues along a fixed stress path, σ^{v} is a unique function of instantaneous values of ε^{ir} and $\dot{\varepsilon}^{ir}$, independent of previous loading history. The term "new" of the model name comes from that, with the original isotach model (Suklje, 1969), the stress σ (therefore σ^{v}) is a function of instantaneous strain rate, $\dot{\varepsilon}=\partial\varepsilon/\partial t$, not $\dot{\varepsilon}^{ir}$. This difference results into significant differences in the model behaviour, in particular during stress relaxation with $\dot{\varepsilon}=0$ and immediately after a step change in $\dot{\varepsilon}$ during otherwise ML at a constant $\dot{\varepsilon}$ (Tatsuoka et al., 1999a).

It was then found that the viscous properties of clean sand (i.e., uniform sand) cannot be properly described by the new isotach model (Eqs. (2) and (3)). For example, Fig. 2(a) shows part of the results from a series of drained PSC tests performed by increasing the effective vertical (axial) stress, σ'_{v}, at a constant effective confining pressure (i.e., horizontal stress) equal to $\sigma'_{h}=392$ kPa on saturated specimens of a clean sand (batch A of RF Hostun sand; a French sand with $D_{50}=0.31$ mm, $U_{c}=1.94$, $G_{s}=2.65$,

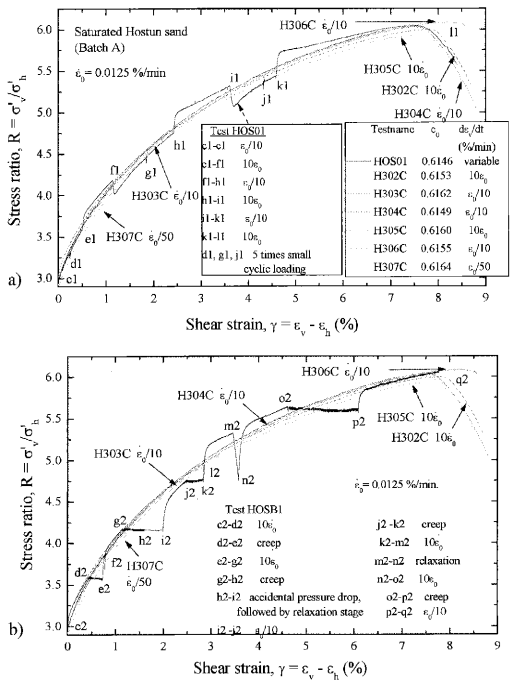

Fig. 2. Relationships between $R=\sigma'_v/\sigma'_h$ and $\gamma=\varepsilon_v-\varepsilon_h$ from drained PSC tests ($\sigma'_h=392$ kPa) at different axial strain rates: a) a test with step changes in the constant strain rate and b) a test in which sustained loading and stress relaxation were performed, saturated Hostun sand (batch A) (Matsushita et al., 1999; Tatsuoka et al., 1999a, 2000)

$e_{max}=0.95$ and $e_{min}=0.55$). Hostun sand is a quartz-rich sub-angular poor-graded medium-sized sand, like Toyoura sand. σ'_v and σ'_h are the major and minor effective principal stresses. ε_v is the vertical (axial) strain, equal to the major principal strain, and ε_h is the horizontal (lateral) strain, equal to the minor principal strain. The specimens were rectangular-prismatic (20 cm high, 16 cm long and 8 cm wide in the σ'_h direction) with well-lubricated top and bottom ends and σ'_2 surfaces. The specimens were prepared by pluviating air-dried sand particles through air and then made saturated. The initial void ratios, e_0, measured at an isotropic stress state when $\sigma'_v=\sigma'_h=29$ kPa were nearly the same among these specimens. The specimens were anisotropically consolidated at a constant principal stress ratio $R=\sigma'_v/\sigma'_h=3.0$ and at a constant axial strain rate, $\dot{\varepsilon}_v=0.0125\%/\text{min}$ from the initial stress state at $\sigma'_h=29$ kPa towards the final stress state at $\sigma'_h=392$ kPa. Then, drained PSC tests were performed. $\dot{\varepsilon}_0$ means the basic axial strain rate, equal to $0.0125\%/\text{min}$. Continuous ML were applied to six specimens at constant axial strain rates, $\dot{\varepsilon}_v$, that were different by a factor of up to 500 (tests H302C through H307C). In another test (HOS01), the axial strain rate was changed stepwise several times by a factor of 100 during otherwise ML at a constant $\dot{\varepsilon}_v$. It may be seen from Fig. 2(a) that the relationships between $R=\sigma'_v/\sigma'_h$ and the shear strain, $\gamma=\varepsilon_v-\varepsilon_h$, from the tests performed at different constant $\dot{\varepsilon}_v$s are essentially independent of $\dot{\varepsilon}_v$. Small effects of $\dot{\varepsilon}_v$ on the stress-strain behaviour were observed only immediately after the start of PSC loading from $R=3.0$ (Matsushita et al., 1999). When based on only the results from tests H302C through H307C, one may consider that the viscous property of Hostun sand is utterly insignificant.

In test HOS012, however, the $R=\sigma'_v/\sigma'_h$ value increases or decreases at a very high rate immediately after $\dot{\varepsilon}_v$ increases or decreases stepwise by a factor of 100 (Fig. 2(a)), which should be attributed to the viscous property of sand. Then, as long as ML continues at a changed strain rate, the stress-strain curve exhibits a marked change in the tangent modulus and the stress-strain curve gradually converges into the essentially unique stress-strain curve that is obtained by continuous ML at any constant strain rate.

Moreover, in Fig. 2(b), the R-γ relation from another test (test HOSB1), in which several sustained loading tests and one stress relaxation test were performed during otherwise ML at a constant strain rate, is compared with those from tests H302C through H307C. It may be seen that significant creep deformation and stress relaxation took place in test HOSB1, which should also be attributed to the viscous property of sand.

In these tests, the stress, σ, is not uniquely controlled by the instantaneous values of ε^{ir} and $\dot{\varepsilon}^{ir}$, not as indicated by Eq. (3). Similar peculiar trends of viscous behaviour have been observed in other PSC tests on air-dried Hostun sand and saturated Toyoura sand (as shown later in this paper), in the torsional shear tests on air-dried Hoston sand (Di Benedetto et al., 2001), in the triaxial compression tests (TC tests) on water-saturated and air-dried Toyoura sand (Matsushita et al., 1999; Nawir et al., 2003 a and b) and in the triaxial compression and extension tests on water saturated fine silica sand (Kiyota et al., 2005). The trends of viscous behaviour seen from Figs. 2(a) and (b) are therefore not unique to these drained PSC tests on saturated Hostun sand.

Then, Di Benedetto et al. (2002) and Tatsuoka et al. (2002) modified Eq. (2) to describe such a decay of viscous effect with an increase in ε^{ir} as described above:

$$\sigma^v=\int_{\tau=\varepsilon_1^{ir}}^{\varepsilon^{ir}}[d\sigma^v]_{(\tau,\varepsilon^{ir})}=\int_{\tau=\varepsilon_1^{ir}}^{\varepsilon^{ir}}[d\sigma^v]_{(\tau)}\cdot g_{decay}(\varepsilon^{ir}-\tau)$$
$$=\int_{\tau=\varepsilon_1^{ir}}^{\varepsilon^{ir}}[d\{\sigma^f\cdot g_v(\dot{\varepsilon}^{ir})\}]_{(\tau)}\cdot g_{decay}(\varepsilon^{ir}-\tau) \quad (5)$$

where σ^v is the current viscous stress component (when $\varepsilon^{ir}=\varepsilon^{ir}$); and the term $[d\sigma^v]_{(\tau,\varepsilon^{ir})}$ is the viscous stress increment that developed in the past when $\varepsilon^{ir}=\tau$ and has decayed until the present (when $\varepsilon^{ir}=\varepsilon^{ir}$). $[d\sigma^v]_{(\tau)}$ is the viscous stress increment that developed following Eq. (2) when $\varepsilon^{ir}=\tau$, equal to $[d\{\sigma^f\cdot g_v(\dot{\varepsilon}^{ir})\}]_{(\tau)}$; ε_1^{ir} is the strain at the start of integration, where $\sigma^v=0$; and $g_{decay}(\varepsilon^{ir}-\tau)$ is the decay function, given as follows (Tatsuoka et al., 2000; Di Benedetto et al., 2002):

$$g_{decay}(\varepsilon^{ir}-\tau)=r_1^{(\varepsilon^{ir}-\tau)} \quad (6a)$$

where r_1 is a positive constant smaller than unity. Although other forms that are different from Eq. (6a) can describe the decay of σ^v with ε^{ir}, the available experimental results support this form of equation, while the power form has a fundamental advantage over the other forms

as described later in this paper. The physical meaning of r_1 of Eq. (6a) can be readily seen by rewriting to:

$$g_{\text{decay}} = (0.5)^{(\varepsilon^{\text{ir}} - \tau)/H} \tag{6b}$$

where H is the irreversible strain increment, ε^{ir}-τ, by which $[d\sigma^{\text{v}}]_{(\tau)}$ becomes half as ML continues. The relationship between the parameters r_1 and H is given by:

$$r_1 = \left(\frac{1}{2}\right)^{1/H} \quad ; \quad \text{or} \quad H = \frac{\log(1/2)}{\log(r_1)} \tag{6c}$$

When $r_1 = 1.0$, H becomes infinitive. On the other hand, when $r_1 = 0$, H becomes zero.

When $r_1 = 1.0$, Eq. (5) returns to Eq. (2) (the new isotach model). By this decay feature (Eqs. (6a) and (6b)), the effects of irreversible strain rate, $\dot{\varepsilon}^{\text{ir}} = \partial\varepsilon^{\text{ir}}/\partial t$, and its rate (i.e., irreversible strain acceleration), $\ddot{\varepsilon}^{\text{ir}} = \partial^2\varepsilon^{\text{ir}}/\partial t^2$, on σ^{v} becomes non-persistent, or temporary, during subsequent ML. The new model is called the TESRA model according to this property (i.e., temporary effects of irreversible strain rate and irreversible strain acceleration on the viscous stress component). As demonstrated by Di Benedetto et al. (2002) and Tatsuoka et al. (2002), when r_1 is less than unity, the value of σ^{v} could become either positive or zero or negative depending on recent loading history even when $\dot{\varepsilon}^{\text{ir}}$ has been kept positive.

Figure 3(a) shows the measured R-ε_{v} relation from a drained PSC test on water-saturated Toyoura sand (a Japanese sand with $D_{50} = 0.18$ mm, $U_{\text{c}} = 1.64$, $G_{\text{s}} = 2.65$, $e_{\max} = 0.99$ and $e_{\min} = 0.62$). In this test, the axial strain rate, $\dot{\varepsilon}_{\text{v}}$, was decreased and increased at a constant rate for some axial strain range, respectively, two times and one sustained loading test was performed during otherwise ML at a constant $\dot{\varepsilon}_{\text{v}}$. The test result is compared with the simulation obtained by directly integrating the Eq. (5) using the parameters presented in the figure (not by the FEM method). The procedure to obtain the model parameters is explained in Di Benedetto et al. (2002). The integration was made based on the measured time history of irreversible axial strain rate, $\dot{\varepsilon}_{\text{v}}^{\text{ir}}$, except for the sustained loading stage, at which the integration was made under the condition that $\dot{\sigma} = 0$. The stiffness immediately after the start of PSC loading from $R = 3.0$ is relatively large. This was due to a sudden increase in the axial strain rate from a low value equal to 0.0125%/min at the end of anisotropic compression at $R = 3.0$ to a constant value equal to about 0.07%/min. Figure 3(b) shows the measured time history of axial strain and its simulation. It may be seen from Figs. 3(a) and 3(b) that all these observed viscous features are well simulated by the TESRA model.

In the present study, the TESRA model was implemented into an existing non-linear elasto-plastic FE code (Siddiquee and Tatsuoka, 2001; Siddiquee et al., 1999, 2001). Some specific considerations were made on the relevant choice of the internal variable for loading rates, which is the key for the success of this implementation. The FE code enriched with the TESRA model were validated by simulating the shear stress—shear (or axial) strain relations from drained PSC tests on sand, including the one presented in Fig. 3.

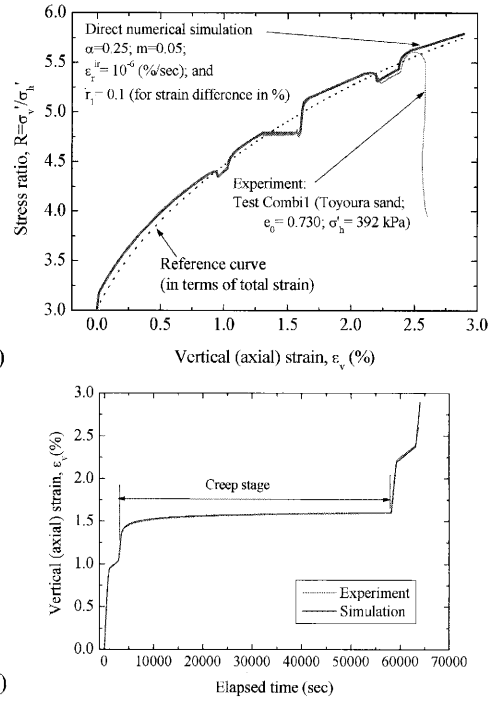

Fig. 3. a) Measured stress ratio—axial strain relation and b) measured time history of axial strain from a drained PSC test (Combi 1) on Toyoura and their direct simulations by the TESRA model (Di Benedetto et al., 2002)

IMPLEMENTATION OF 'TESRA' MODEL INTO A FE CODE

Formulation of TESRA Model

Equation (2) can be rewritten as:

$$\sigma^{\text{v}} = \int_{\tau=\varepsilon_i^{\text{ir}}}^{\varepsilon^{\text{ir}}} \left[\left(\frac{\partial\sigma^{\text{f}}}{\partial\varepsilon^{\text{ir}}} \right) \cdot g_{\text{v}}(\dot{\varepsilon}^{\text{ir}}) + \sigma^{\text{f}} \cdot \left(\frac{\partial g_{\text{v}}(\dot{\varepsilon}^{\text{ir}})}{\partial\dot{\varepsilon}^{\text{ir}}} \right) \cdot \frac{\ddot{\varepsilon}^{\text{ir}}}{\dot{\varepsilon}^{\text{ir}}} \right]_{(\tau)} \cdot d\tau \tag{7}$$

where the term $[(\partial\sigma^{\text{f}}/\partial\varepsilon^{\text{ir}}) \cdot g_{\text{v}}(\dot{\varepsilon}_{\text{v}}^{\text{ir}}) \cdot d\varepsilon^{\text{ir}}]_{(\tau)}$ represents the component of $[d\sigma^{\text{v}}]_{(\tau)}$ that develops by $d\varepsilon^{\text{ir}}$ when $\varepsilon^{\text{ir}} = \tau$ during ML at a constant $\dot{\varepsilon}$; and the second term $[\sigma^{\text{f}} \cdot (\partial g_{\text{v}}(\dot{\varepsilon}^{\text{ir}})/\partial\dot{\varepsilon}^{\text{ir}}) \cdot d\dot{\varepsilon}^{\text{ir}}]_{(\tau)}$ represents the component of $[d\sigma^{\text{v}}]_{(\tau)}$ that develops by the increment of irreversible strain rate, $d\dot{\varepsilon}^{\text{ir}}$, at a fixed ε^{ir} $(= \tau)$. To derive Eq. (7), $d\dot{\varepsilon}^{\text{ir}} = \ddot{\varepsilon}^{\text{ir}} \cdot dt = \ddot{\varepsilon}^{\text{ir}} \cdot (d\varepsilon^{\text{ir}}/\dot{\varepsilon}^{\text{ir}})$ was used. By substituting Eq. (6a) into Eq. (5) while referring to Eq. (7), we obtain:

$$\sigma^{\text{v}} = \int_{\tau=\varepsilon_i^{\text{ir}}}^{\varepsilon^{\text{ir}}} \left[\left(\frac{\partial\sigma^{\text{f}}}{\partial\varepsilon^{\text{ir}}} \right) \cdot g_{\text{v}}(\dot{\varepsilon}^{\text{ir}}) + \sigma^{\text{f}} \cdot \left(\frac{\partial g_{\text{v}}(\dot{\varepsilon}^{\text{ir}})}{\partial\dot{\varepsilon}^{\text{ir}}} \right) \cdot \frac{\ddot{\varepsilon}^{\text{ir}}}{\dot{\varepsilon}^{\text{ir}}} \right]_{(\tau)} \cdot r_1^{(\varepsilon^{\text{ir}} - \tau)} \cdot d\tau \tag{8}$$

When directly using Eq. (8) to obtain the current value of σ^{v}, an integration procedure should be repeated for every small increment of ε^{ir} to update the value of σ^{v}.

In Eqs. (7) and (8), the irreversible strain acceleration, $\ddot{\varepsilon}^{\text{ir}}$, is used. Inclusion of a strain acceleration term in the viscosity formulation does not mean that inertia force is incorporated in the proposed constitutive model, which is indeed totally irrelevant, making the constitutive equation totally non-objective. The strain rate and strain acceleration terms are used only in the incremental

viscosity calculation generating viscous stress increments as the material property. It should also be noted that, in the laboratory stress-strain tests that provided the data that were used to develop the proposed model, the inertia force of the testing system and specimen due to acceleration was utterly negligible (Matsushita et al., 1999).

As an incremental solution technique is usually employed in the FEM, it is extremely difficult, if not impossible, to perform to obtain a solution for a given boundary value problem by a FE code in which Eq. (8) is implemented. Tatsuoka et al. (2002) showed that Eq. (8) can be transformed into the following incremental form without losing accuracy for a sufficiently small increment:

$$\begin{aligned}\sigma^{\mathrm{v}} &\cong \int_{\tau=\varepsilon_1^{\mathrm{ir}}}^{\varepsilon^{\mathrm{ir}}-\Delta\varepsilon^{\mathrm{ir}}} [d\sigma^{\mathrm{f}}\cdot g_{\mathrm{v}}(\dot{\varepsilon}^{\mathrm{ir}})]_{(\tau)}\cdot g_{\mathrm{decay}}(\varepsilon^{\mathrm{ir}}-\tau)\cdot d\tau+\Delta\sigma^{\mathrm{v}} \\ &= \left[\int_{\tau=\varepsilon_1^{\mathrm{ir}}}^{\varepsilon^{\mathrm{ir}}-\Delta\varepsilon^{\mathrm{ir}}} [d\sigma^{\mathrm{f}}\cdot g_{\mathrm{v}}(\dot{\varepsilon}^{\mathrm{ir}})]_{(\tau)}\cdot r_1^{(\varepsilon^{\mathrm{ir}}-\tau-|\Delta\varepsilon^{\mathrm{ir}}|)}\cdot d\tau\right]\cdot r_1^{|\Delta\varepsilon^{\mathrm{ir}}|}+\Delta\sigma^{\mathrm{v}} \\ &= [\sigma^{\mathrm{v}}]_{(\varepsilon^{\mathrm{ir}}-\Delta\varepsilon^{\mathrm{ir}})}\cdot r_1^{|\Delta\varepsilon^{\mathrm{ir}}|}+\Delta\{\sigma^{\mathrm{f}}\cdot g_{\mathrm{v}}(\dot{\varepsilon}^{\mathrm{ir}})\}\cdot r_1^{|\Delta\varepsilon^{\mathrm{ir}}|/2} \end{aligned} \tag{9}$$

where $[\sigma^{\mathrm{v}}]_{(\varepsilon^{\mathrm{ir}}-\Delta\varepsilon^{\mathrm{ir}})}$ is the viscous stress at one step immediately before, where the irreversible strain is equal to $\varepsilon^{\mathrm{ir}}-\Delta\varepsilon^{\mathrm{ir}}$; $\Delta\varepsilon^{\mathrm{ir}}$ is the irreversible strain increment taking place between one step immediately before and the current step, which is positive for loading; and $\Delta\{\sigma^{\mathrm{f}}\cdot g_{\mathrm{v}}(\dot{\varepsilon}^{\mathrm{ir}})\}$ is the difference in $\sigma^{\mathrm{f}}\cdot g_{\mathrm{v}}(\dot{\varepsilon}^{\mathrm{ir}})$ between the current step and one step immediately before, given as:

$$\Delta\{\sigma^{\mathrm{f}}\cdot g_{\mathrm{v}}(\dot{\varepsilon}^{\mathrm{ir}})\} = [\sigma^{\mathrm{f}}\cdot g_{\mathrm{v}}(\dot{\varepsilon}^{\mathrm{ir}})]_{[\varepsilon^{\mathrm{ir}}]} - [\sigma^{\mathrm{f}}\cdot g_{\mathrm{v}}(\dot{\varepsilon}^{\mathrm{ir}})]_{[\varepsilon^{\mathrm{ir}}-\Delta\varepsilon^{\mathrm{ir}}]} \tag{10}$$

So, for given values of $[\sigma^{\mathrm{v}}]_{(\varepsilon^{\mathrm{ir}}-\Delta\varepsilon^{\mathrm{ir}})}$ as well as the known parameters representing the loading history between one step immediately before and the current step (i.e., the values of $\Delta\varepsilon^{\mathrm{ir}}$ and Δt or $\dot{\varepsilon}^{\mathrm{ir}}=\Delta\varepsilon^{\mathrm{ir}}/\Delta t$), the values of $\varepsilon^{\mathrm{ir}}$ and σ^{v} at the current state (where $\varepsilon^{\mathrm{ir}}=\varepsilon^{\mathrm{ir}}$) can be obtained by Eqs. (9) and (10) without repeating the integration from the start of loading. Repeating this incremental procedure from the start of loading, the whole stress-strain-time relation for any given history of strain or stress can be obtained. In the present FEM simulation, a one-step Euler type integration was employed with Eq. (9). This method is very fast despite that the use of Eq. (9) has some restrictions in accuracy and stability.

Implementation into a FE Code

The TESRA model was implemented into an existing non-linear elasto-plastic FE code (Siddiquee and Tatsuoka, 2001; Siddiquee et al., 1999, 2001), which was developed based on the matrix-free dynamic relaxation (DR) technique that was highly optimized for very fast and accurate computation of highly non-linear equations emerging from material non-linearity. Due to the inherent features of the DR technique, the following steps were revised carefully when implementing the TESRA model into the FE code.

Firstly, as the governing equations of motion are integrated by the solution technique of the DR method, no other integration is apparently necessary in the time domain even when dealing with problems including loading rate effects due to material viscosity. However, the use of a fictitious diagonal mass matrix in the DR technique to obtain solutions efficiently may affect the accuracy of the solution when incorporating material property into the material stress-strain model. Then, a real mass should be used when actually solving any problem including viscous effects.

Secondly, the basic controlling variable in the present version of the TESRA model is the irreversible shear strain rate at any step of calculation. Then, the relevant parameter for the rate variable should be chosen in the non-linear FEM analysis so that accurate irreversible shear strain rates can be obtained. With the present FEM analysis based on an isotropic hardening model, the rate of the effective plasticity parameter, κ, defined as follows, becomes the primary candidate for the rate variable.

$$\kappa = \sqrt{\sum_{ij}(\varepsilon_{ij}^{\mathrm{dev}})^2} \tag{11}$$

where $\varepsilon_{ij}^{\mathrm{dev}}$ is the deviatoric irreversible strain, which has some advantages in that this quantity is a scalar quantity and it is already being calculated in the FE analysis. However, as this quantity is always positive whether the loading condition is 'loading' or 'unloading', it cannot be used in the analysis of the unloading process. One alternative is the rate of maximum irreversible shear strain, which is also being calculated in any FE analysis. So the maximum irreversible shear strain and its rate, given below, are used in the present formulation:

$$\gamma^{\mathrm{ir}} = \varepsilon_1^{\mathrm{ir}} - \varepsilon_3^{\mathrm{ir}}; \quad \dot{\gamma}^{\mathrm{ir}} = d\gamma^{\mathrm{ir}}/dt \tag{12}$$

$\gamma^{\mathrm{ir}}=\varepsilon_1^{\mathrm{ir}}-\varepsilon_3^{\mathrm{ir}}$ is equal to $\varepsilon_{\mathrm{v}}^{\mathrm{ir}}-\varepsilon_{\mathrm{h}}^{\mathrm{ir}}$ in the present case. Then, loading/neutral/unloading conditions are determined as follows: 1) $\dot{\gamma}^{\mathrm{ir}}>0$: loading; 2) $\dot{\gamma}^{\mathrm{ir}}=0$: neutral loading; and 3) $\dot{\gamma}^{\mathrm{ir}}<0$: unloading.

Thirdly, a relevant stress parameter should be chosen when evaluating the viscous stress, σ^{v}. In the present study, based on the experimental results (Di Benedetto et al., 2002), the effective principal stress ratio, $R=\sigma_1'/\sigma_3'$, was chosen as the stress parameter, σ, in Eqs. (9) and (10) for primary ML at a fixed confining pressure. Nawir et al. (2003a, b) showed that it is also the case for stress paths along different confining pressures and when the confining pressure is changing during ML. Then, it is considered that Eqs. (9) and (10) can also be applied to general ML stress conditions where σ_1' and σ_3' change arbitrarily.

Pseudo-Algorithm

The following pseudo-algorithm was developed revising the original solution technique of the DR method not including viscous effects. That is, the total stress (i.e., σ in Eq. (1)) at equilibrium is calculated at two levels of integration as follows.

At the first level of integration, incremental elasto-plastic equations are solved inside the "return mapping algorithm" (Ortiz and Simo, 1986), where the stress is returned to the growing yield surface while fulfilling the consistency condition (abiding by the flow rule). At each step of return mapping iteration, when necessary, the second level of integration is made, where the stress is

returned to the inviscid yield surface with an incremental integration based on the TESRA model while calculating the viscous stress. This scheme presented in Fig. 4 and described below.

G1. Calculation of trial strain

G2. Calculation of total stress increment as an elastic solution based on the hypo-elastic constitutive law (Hoque and Tatsuoka, 1998):

$$E_h = E_0 \cdot \sigma_h^n; \quad E_v = E_0 \cdot \sigma_v^n;$$
$$\nu_{vh} = \nu_0 \cdot (\sigma_v/\sigma_h)^{n/2}; \quad \nu_{hv} = \nu_0 \cdot (\sigma_h/\sigma_v)^{n/2} \tag{13}$$

G3. Execution of "return mapping" scheme:

(1) It is checked whether the current total stress component is over-shooting the instantaneous yield surface (described in the total stress component).

(2) If the current total stress component lies above the instantaneous yield surface, the total stress component should be integrated back to the yield surface by iterations according to the "return mapping" scheme.

(3) The elasto-plastic solution (without viscous effects) is obtained. That is, applying the plastic consistency conditions and the flow rule, each trial total stress component is integrated back to the inviscid yield surface, f^f, as:

$$df^f(\sigma_{ij}, \kappa) = 0, \quad d\varepsilon_{ij}^p = \lambda \frac{\partial \Psi}{\partial \sigma_{ij}} \tag{14}$$

where Ψ is the plastic potential function originally defined in the inviscid stress, which is equal to the total stress at this stage.

(4) For the calculation of "return mapping" starting from step (1), the current inviscid stress parameter, R^f ($R = \sigma_1'/\sigma_3'$), is calculated based on the material model (the material inviscid stress ratio—maximum irreversible shear strain relation).

(5) While calculating the current inviscid stress at step (4), the viscous stress increment is also calculated by the following steps:

V1: The irreversible shear strain increment (Eq. (12)) is calculated.

V2: For a known time increment obtained from the information of applied loading history, the irreversible shear strain rate is calculated. The previous rate is known as it has been saved at the end of previous step.

V3: By following Eq. (10), which is derived from Eq. (5), the viscous stress increment, $\Delta\{\sigma^f \cdot g_v(\dot{\varepsilon}^{ir})\}$, in terms of ΔR^v ($R = \sigma_1'/\sigma_3'$) is calculated.

V4: By following Eq. (9), by adding the present viscous stress increment, $\Delta\{\sigma^f \cdot g_v(\dot{\varepsilon}^{ir})\}$, to the saved viscous stress at the previous step while using the appropriate decay parameter, the present viscous stress, σ^v, is obtained.

V5: The new total stress component, σ, is obtained by adding the viscous component, σ^v, to the inviscid stress, σ^f, that has been obtained from the reference stress-strain relation.

(6) Now, it is checked whether the new total stress, $\sigma = \sigma^f + \sigma^v$, satisfies the current yield surface (described in σ). If it is not, iteration continues by returning to step (2).

G4. Element stresses are integrated to form nodal forces and compared with the applied load. The iteration continues, starting from step G1 again, until the global equilibrium is reached.

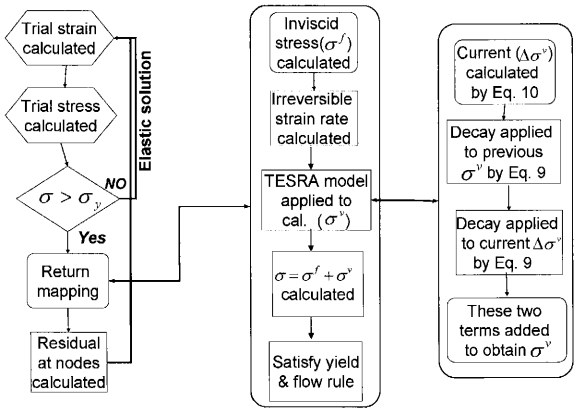

Fig. 4. Implementation of the "TESRA" model into a FEM code

It is to be noted that the plastic potential, Ψ, (Eq. (14)) is defined in terms of inviscid stresses in the numerical method that is proposed in the framework of the three-component model. This feature is different from the over-stress model (Perzyna, 1963), in which the current plastic potential is defined in terms of instantaneous total stresses while the inviscid stress is not evaluated.

NUMERICAL SIMULATION BY FEM

Problem Definition

A 10 cm × 10 cm one-element configuration was devised (Fig. 5(a)). To confirm whether the present FEM simulation can be applied to general boundary value problems, multi-element PSC test simulations were also performed using the mesh presented in Fig. 5(b) and the results were compared with those by one-element simulations. The top and bottom ends of the domain are supported with rollers to simulate a high quality of lubrication in the physical PSC tests.

In each simulation case, the reference stress-strain curve was first simulated with some trial and error by the FEM simulation without including any viscous component. The reference stress-strain relation thus obtained was used as the inviscid stress-strain relation in the FEM simulation. The FEM simulation was made at a very slow strain rate (10^{-6} %/s).

Material Model

The generalized elasto-plastic isotropic strain-hardening and softening model used in the present study takes

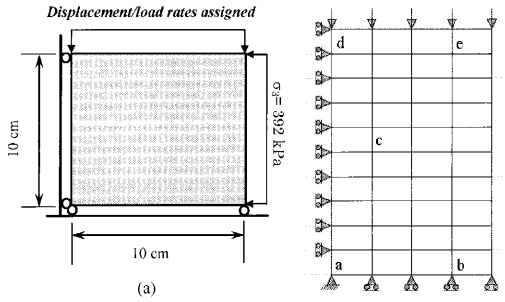

Fig. 5. a) One-element and b) multi-element for FEM simulation of PSC test (not to the scale, one-fourth of the whole domain, 8 cm × 20 cm, is presented here)

into account strain localization associated with shear banding by introducing a characteristic width of shear band in the additive elasto-plastic decomposition of strain.

A generalized hyperbolic equation (GHE) (Tatsuoka et al., 1993) is used as the growth function of the yield surface of the generalized Mohr-Coulomb type, given by:

$$\Phi = -\eta I_1 + \frac{1}{g(\theta)}\sqrt{J_2} - K \tag{15}$$

where I_1 is the first stress invariant (i.e., hydrostatic stress component, positive in compression); and J_2 is the second deviatoric stress invariant (i.e., the deviatoric stress). The growth function is explained in detail in Siddiquee et al. (1999, 2001a and b). The function $g(\theta)$ in Eq. (15) is the Lode angle function, defined as (Nayak et al., 1972);

$$g(\theta) = \frac{3 - \sin\phi_{mob}}{2\sqrt{3}\cos\theta - 2\sin\theta\sin\phi_{mob}} \tag{16}$$

In Eq. (15), η is the magnitude of the deviatoric stress at $\theta = 30°$ (on the π-plane), which is related to the mobilized angle of friction, φ_{mob}, as;

$$\eta = \frac{2\sin\phi_{mob}}{\sqrt{3}(3 - \sin\phi_{mob})} \tag{17}$$

Using the viscosity function incrementally, the viscous component of effective principal stress ratio, R^v, is calculated for a given inviscid stress ratio R^f, from which the inviscid component of φ_{mob} is obtained. The sum of these two produces the total stress ratio, R, from which the value of φ_{mob} is obtained.

The plastic potential, Ψ, (Eq. (14)) is defined as;

$$\Psi = -\alpha' I_1 + \sqrt{J_2} - K = 0 \tag{18}$$

This plastic potential function, of the Drucker-Prager type, is similar to the yield function except that $g(\theta)$ in Eq. (15) is equal to unity in Eq. (18). Equation (18) is employed so as to have differentiability at all stress states. The factor α' depends on the type of analysis. The factor α' used in the present analysis under plane strain conditions is linked to the mobilized dilatancy angle ν as;

$$\alpha' = \frac{\tan\nu}{\sqrt{9 + 12\tan^2\nu}} \tag{19}$$

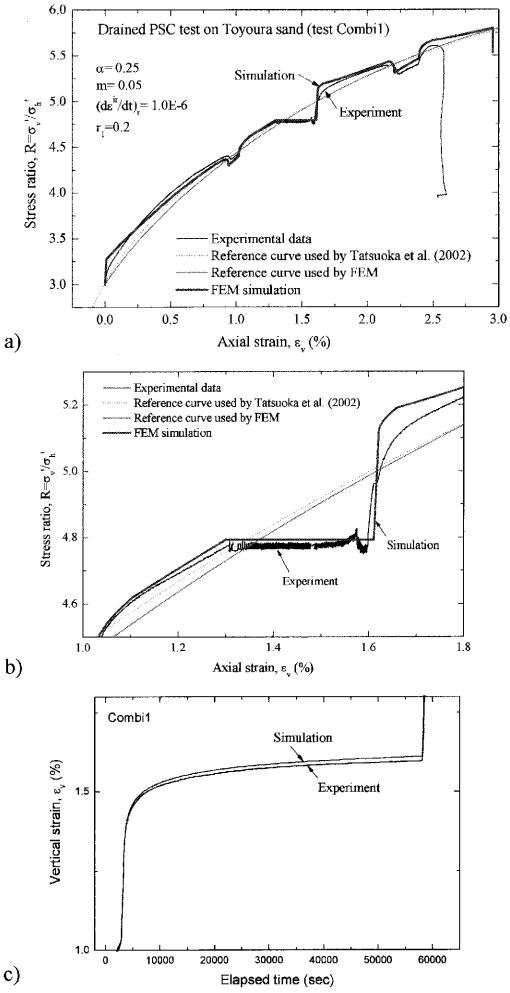

Fig. 6. Test result and FEM simulation of PSC test "Combi1" on Toyoura sand (basic $\dot{\varepsilon}_v$ = 0.07 and 0.035%/min refer to Fig. 3): a) stress ratio—axial strain relation (simulation using single element), b) a zoom-up and c) time history of shear strain (simulation using single element)

$$\nu = \arcsin\left(-\frac{d\varepsilon_1^{ir} + d\varepsilon_3^{ir}}{d\varepsilon_1^{ir} - d\varepsilon_3^{ir}}\right) \tag{20}$$

where $d\varepsilon_1^{ir}$ and $d\varepsilon_3^{ir}$ are the major and minor irreversible principal strain increments (positive in compression), which are linked to each other through the Rowe's stress-dilatancy relation (Rowe, 1962);

$$\frac{\sigma_1'}{\sigma_3'} = -K\left(\frac{d\varepsilon_1^{ir}}{d\varepsilon_3^{ir}}\right) \tag{21}$$

where K is a material constant (equal to 3.5 for Toyoura sand and 3.0 for Huston sand in the present case). As the model has the yield function and plastic potential surface having different forms, it is one of the non-normal plasticity models or non-associated flow models (Vermeer and de Borst, 1984).

FEM SIMULATION OF PSC TEST RESULTS

The results from three drained PSC tests on saturated Toyoura sand (batch E) and two drained PSC tests on air-dried Hostun sand (batch B) that are reported in Di

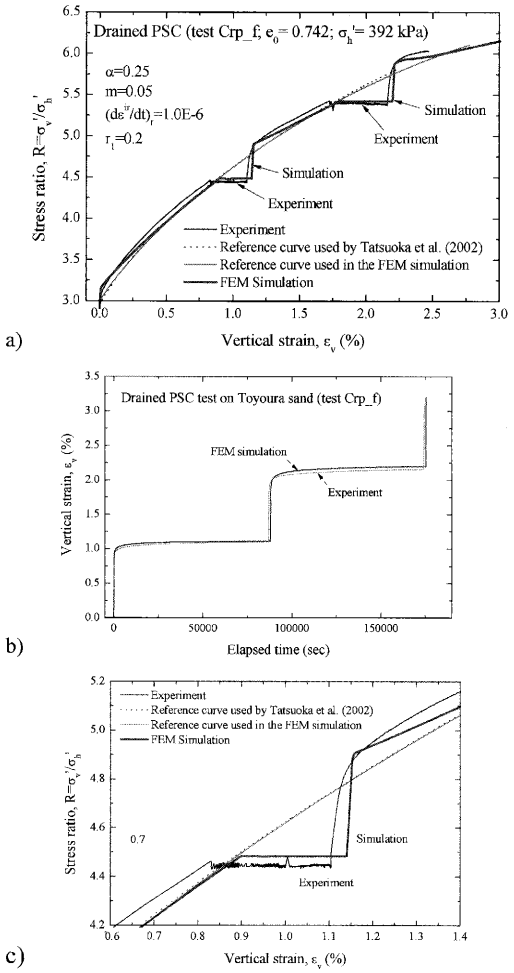

Fig. 7. Test result and FEM simulation (using single element) of PSC test "Crp_f" on Toyoura sand (basic $\dot{\varepsilon}_v = 0.25\%/\text{min}$): a) stress ratio—axial strain relation, b) a zoom-up and c) time history of axial strain

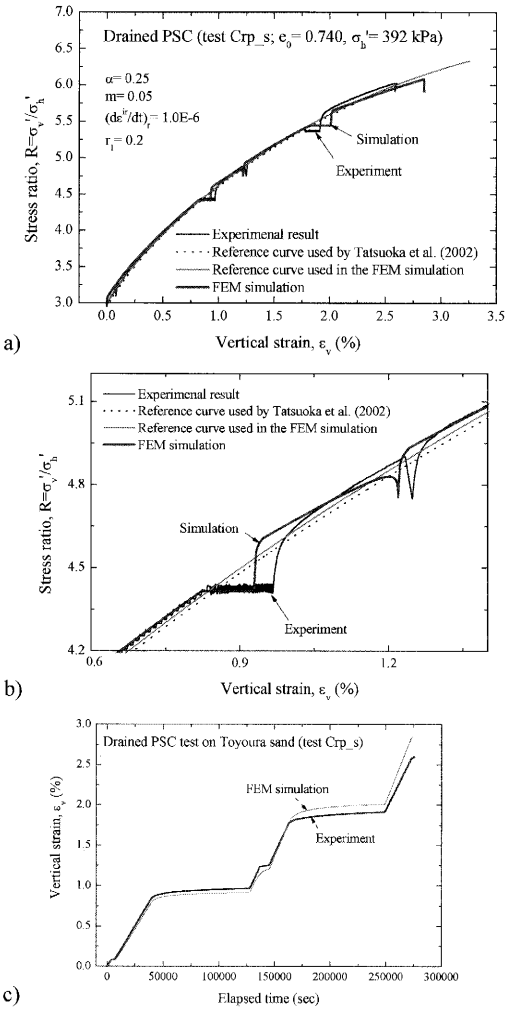

Fig. 8. Test result and FEM simulation (using single element) of PSC test "Crp_s" on Toyoura sand (basic $\dot{\varepsilon}_v = 0.0025\%/\text{min}$): a) stress ratio—axial strain relation, b) a zoom-up and c) time history of axial strain

Benedetto et al. (2002) and Tatsuoka et al. (2002) were simulated by the FEM. In these PSC tests, at several intermediate stages, the axial strain rate $\dot{\varepsilon}_v$ was increased and decreased stepwise or gradually at a constant rate, while sustained loading was applied one or two times during otherwise ML in some tests.

FEM Simulation

The reference stress-strain curve used in the respective FEM simulation is presented in the respective figure presented below. The parameters of the viscosity function (Eq. (4)) used in the FEM simulation are the same as those used by the direct TESRA model simulation reported by Di Benedetto et al. (2002) and Tatsuoka et al. (2002), which are as follows:

1) $\alpha = 0.25$, $m = 0.05$ and $\dot{\varepsilon}_r^{ir} = 0.000001\%/\text{s}$ ($10^{-6}\%/\text{s}$) for Toyoura sand; and
2) $\alpha = 0.25$, $m = 0.04$ and $\dot{\varepsilon}_r^{ir} = 0.000001\%/\text{s}$ for Hostun sand.

For the decay function for the TESRA viscous property (Eq. (6a)), $r_1 = 0.2$ (Toyoura sand) and $r_1 = 0.1$ (Hostun sand), both defined in terms of irreversible shear strain increment in %, were used. It is to be noted that, even for the same PSC test data, the value of r_1 (Eq. (6a)) is larger when based on the shear strain, $\gamma = \varepsilon_v - \varepsilon_h$, than when based on the axial strain, ε_v, due to different decay rates when based on γ and ε_v. For example, Di Benedetto et al. (2002) used $r_1 = 0.2$ and 0.1 in the direct TESRA model simulation of the drained PSC test data of Toyoura sand when based on, respectively, $\gamma = \varepsilon_v - \varepsilon_h$ and ε_v. The parameters of the hypo-elastic model (Eq. (13)) are:

1) $E_0 = 173$ MPa for Toyoura and Hostun sands; and
2) $\nu_0 = 0.17$ and $n = 0.41$ for both Toyoura and Hostun sands.

The FEM simulations were performed by strain control based on the measured time histories of irreversible shear strain, except for sustained loading stages, for which the simulations were performed by stress control with $\dot{\sigma} = 0$ (i.e., $\dot{R} = 0$). The stress ratio—shear (or axial) strain curves and time histories of shear (or axial) strain obtained from the FEM simulation are compared with measured ones in Figs. 6 through 10. Despite that the $R - \varepsilon_v$ relations are presented in Figs. 6, 7 and 8 for Toyoura sand following Di Benedetto et al. (2002), the FEM simulations were performed based on the time

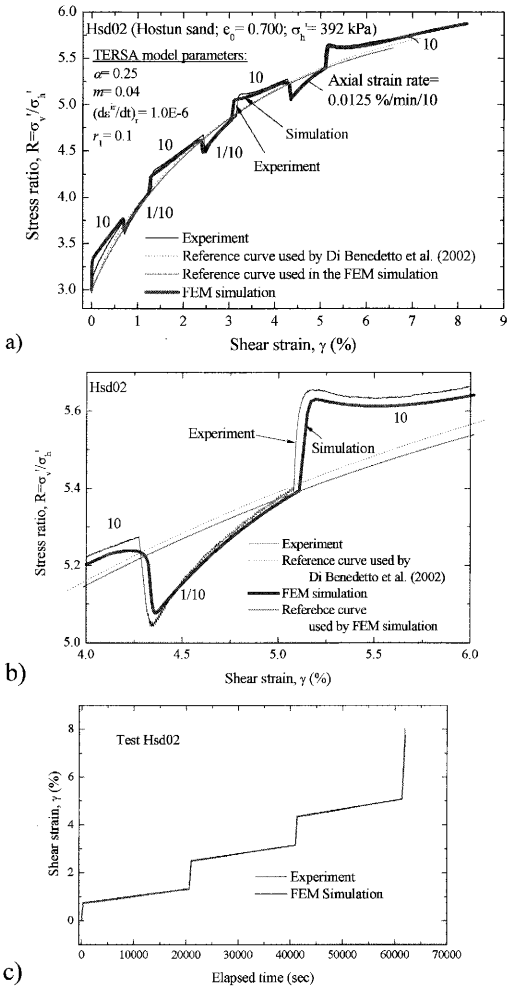

Fig. 9. Test results and FEM simulation (using single element) of PSC test "Hsd02" on Hostun sand (basic $\dot{\varepsilon}_v = 0.0125\%/\text{min}$): a) stress ratio—shear strain relation, b) a zoom-up and c) time history of shear strain (given data for simulation)

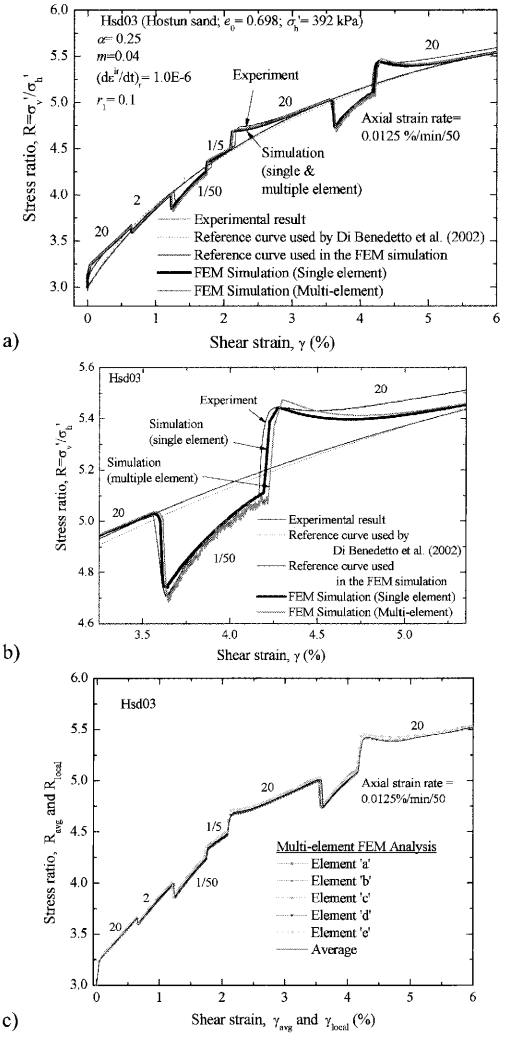

Fig. 10. Test results and FEM simulation of PSC test "Hsd03" on Hostun sand (basic $\dot{\varepsilon}_v = 0.0125\%/\text{min}$): a) stress ratio—shear strain relation (simulation using multi-element and single element), b) a zoom-up (simulation using single element) and c) local relations of stress ratio and shear strains in a multiple-element

histories of irreversible shear strain, γ^{ir}.

The following trends of behaviour may be seen from these figures:

1) In all the PSC tests, the axial strain rate was stepwise increased at the start of PSC loading. Subsequently, during otherwise ML, the axial strain rate was changed gradually at a constant rate in test Combi1 (Fig. 6) and stepwise by a factor of 100 in test Hsd02 (Fig. 9) and by a factor ranging from 10 to 1,000 in test Hsd03 (Fig. 10). Note that the changing rate of irreversible shear strain was always approximately the same as that of axial strain. The behaviour that the stress exhibits gradual and sudden changes upon gradual and sudden changes in the strain rate, including the one immediately after the start of PSC loading, is well simulated.
2) Despite that the basic axial strain rate (therefore, the irreversible shear strain rate) was different by a factor of 100 between test Crp_f (Fig. 7) and test Crp_s (Fig. 8), the stress-strain behaviour gradually became the same as ML at a constant strain rate continued. On the other hand, the creep strain rate was larger when sustained loading started at a larger initial strain rate in test Crp_f than when sustained loading started at a lower initial strain rate in test Crp_s. All these viscous aspects of stress-strain behaviour, including the time histories of strain during sustained loading, were simulated very well by the FEM analysis. In test Crp_s (Fig. 8), a stress relaxation test was performed, which was also well simulated.
3) The results from the FEM simulations carried out on a single-element and a multi-element are essentially the same (Fig. 10). A small difference, as seen in Fig. 10(b), is due to different numerical errors between the single and multiple element analysis. In Fig. 10(c), local stress-strain relations in several representative local elements (indicated in Fig. 5(b)) in the multiple-element analysis are presented. The local stress-strain relations are very similar. The multi-element simulations took longer time than the one-element simulation (about ten times).

The result 3) indicates that the FE code enriched by implementing the TESRA model can be applied to general boundary value problems, in which multiple-element

simulations should be inevitably performed. Results from simulations of such boundary value problems taking into account the effects of the viscous property of sand was reported in Tatsuoka (2004) and will also in the near future by the authors.

The implementation of the new isotach model into a FEM code is much simpler than that of the TESRA model. The implementation of the general TESRA model (Tatsuoka et al., 2002), which simulates the increase in the decay rate of viscous stress with an increase in the irreversible strain, ε^{ir}, into a FE code is also possible by updating the parameter r_1 as a function of instantaneous value of ε^{ir} in Eq. (9).

CONCLUSION

A non-linear three-component model (named the TESRA model), which had been developed to describe the peculiar viscous property of uniform sand, was implemented successfully in a nonlinear elasto-plastic FE code without major modifications to the original code. It is shown in this paper that the FE code enriched by implementing the TESRA model can simulate very well the loading rate effects on the relationships between the shear stress (i.e., the effective principal stress ratio) and the shear strain (and the axial strain) due to the material viscous property observed in a series of drained PSC tests on Toyoura and Hostun sands performed using various loading histories. In particular, the decay of viscous effects with an increase in the strain was simulated successfully. Finally, FEM simulations of PSC tests carried out on both one-element and multi-element provided essentially the same results, although the multi-element simulation took longer time (about ten times).

REFERENCES

1) Di Benedetto, H. (1987): Modélisation du comportement des géomatériaux: application aux enrobés bitumineux et aux bitumes, *Thèse de Docteur d'Etat ès Sciences, INPG-USTMG-ENTPE*, 310 (in French).
2) Di Benedetto, H. and Tatsuoka, F. (1997): Small strain behaviour of geomaterials: modelling of strain effects, *Soils and Foundations*, **37**(2), 127–138.
3) Di Benedetto, H., Sauzeat, C. and Geoffroy, H. (2001): Modelling viscous effects and behaviour in the small strain domains, *Proc. 2nd Int. Symp. on Prefailure Deformation Characteristics of Geomaterials, IS Torino* (eds. by Jamiolkowski et al.), **2**, 1357–1367.
4) Di Benedetto, H., Tatsuoka, F. and Ishihara, M. (2002): Time-dependent shear deformation characteristics of sand and their constitutive modeling, *Soils and Foundations*, **42**(2), 1–22.
5) Hoque, E. and Tatsuoka, F. (1998): Anisotropy in the elastic deformation of materials, *Soils and Foundations*, **38**(1), 163–179.
6) Kiyota, T., Tatsuoka, F. and Yamamuro, J. (2005): Drained and undrained creep characteristics of loose saturated sand and their relation, *GeoFrontier05*, GeoInstitute, Austin, Texas.
7) Kuwano, R. and Jardine, R. J. (2002): On measuring creep behaviour in granular materials through triaxial testing, *Can. Geotech. J.*, **39**, 1061–1074.
8) Lade, P. and Liu, C.-T. (1998): Experimental study of drained creep behavior of sand, *J. Engrg. Mech.*, ASCE, **124**(8), 912–920.
9) Matsushita, M., Tatsuoka, F., Koseki, J., Cazacliu, B., Di Benedetto, H. and Yasin, S. J. M. (1999): Time effects on the pre-peak deformation properties of sands, *Proc. 2nd Int. Conf. on Pre-Failure Deformation Characteristics of Geomaterials, IS Torino '99* (eds. by Jamiolkowski et al.), Balkema, **1**, 681–689.
10) Nawir, H., Tatsuoka, F. and Kuwano, R. (2003a): Experimental evaluation of the viscous properties of sand in shear, *Soils and Foundations*, **43**(6), 13–31.
11) Nawir, H., Tatsuoka, F. and Kuwano, R. (2003b): Viscous effects on the shear yielding characteristics of sand, *Soils and Foundations*, **43**(6), 33–50.
12) Nayak, G. C. and Zienkiewicz, O. C. (1972): Elastic-plastic stress analysis: a generalization for various constitutive relations including strain softening, *Int. J. Num. Meth. Engrg.*, **5**(1), 113–125.
13) Ortiz, M. and Simo, J. C. (1986): An analysis of a new class of integration algorithms for elastoplastic constitutive relations, *Int. J. Num. Meth. Engrg.*, **23**, 353–366.
14) Perzyna, P. (1963): The constitutive equations for work-hardening and rate-sensitive plastic materials, *Proc. Vibrational Problems*, Warsaw, **4**(3), 281–290.
15) Rowe, P. W. (1962): The stress dilatancy relation for static equilibrium of an assembly of particles in contact, *Proc. Royal Society*, London, series A, 500–527.
16) Siddiquee, M. S. A. and Tatsuoka, F. (2001): Modeling time-dependent stress-strain behaviour of stiff geomaterials and its applications, *Proc. 10th Int. Conf. Comput. Meth. Adv. Geomech. (IACMAG)*, January 7–12, Tucson, Arizona.
17) Siddiquee, M. S. A., Tanaka, T., Tatsuoka, F., Tani, K. and Morimoto, T. (1999): FEM simulation of scale effect in bearing capacity of strip footing on sand, *Soils and Foundations*, **39**(4), 91–109.
18) Siddiquee, M. S. A., Tatsuoka, F., Tanaka, T., Tani, K., Yoshida, K. and Morimoto, T. (2001): Model tests and FEM simulation of some factors affecting the bearing capacity of footing on sand, *Soils and Foundations*, **41**(2), 53–76.
19) Suklje, L. (1969): Rheological aspects of soil mechanics, *Wiley-Interscience*, London.
20) Tatsuoka, F. (2004): Effects of viscous properties and ageing on the stress-strain behaviour of geomaterials, *Proc. GI-JGS Workshop* (eds. by Yamamuro and Koseki), ASCE Geotechnical SPT (to appear).
21) Tatsuoka, F. and Kohata, Y. (1995): Stiffness of hard soils and soft rocks in engineering applications, Keynote Lecture, *Proc. Int. Symp. Pre-Failure Deformation of Geomaterials* (eds. by Shibuya et al.), Balkema, **2**, 947–1063.
22) Tatsuoka, F., Siddiquee, M. S. A., Park, C.-S., Sakamoto, M. and Abe, F. (1993): Modelling stress-strain relations of sand, *Soils and Foundations*, **33**(2), 60–81.
23) Tatsuoka, F., Jardine, R. J., Lo Presti, D., Di Benedetto, H. and Kodaka, T. (1999): Characterising the pre-failure deformation properties of geomaterials, Theme Lecture for the Plenary Session No. 1, *Proc. XIV IC*, September 1997, Hamburg, **4**, 2129–2164.
24) Tatsuoka, F., Santucci de Magistris, F., Hayano, K., Momoya, Y. and Koseki, J. (2000): Some new aspects of time effects on the stress-strain behaviour of stiff geomaterials, Keynote Lecture, *The Geotechnics of Hard Soils—Soft Rocks, Proc. 2nd Int. Conf. on Hard Soils and Soft Rocks*, Napoli, 1998 (eds. by Evamgelista and Picarelli), Balkema, **2**.
25) Tatsuoka, F., Uchimura, T., Hayano, K., Di Benedetto, H., Koseki, J. and Siddiquee, M. S. A. (2001): Time-dependent deformation characteristics of stiff geomaterials in engineering practice, Theme Lecture, *Proc. 2nd Int. Conf. Pre-failure Deformation Characteristics of Geomaterials*, Torino, 1999, Balkema (eds. by Jamiolkowski et al.), **2**, 1161–1262.
26) Tatsuoka, F., Ishihara, M., Di Benedetto, H. and Kuwano, R. (2002): Time-dependent shear deformation characteristics of geomaterials and their simulation, *Soils and Foundations*, **42**(2), 103–129.
27) Vermeer, P. A. and de Borst, R. (1984): Non-associated plasticity for soils, concrete and rock, *Heron*, **29**(3), 1–64.
28) Yasin, S. J. M. and Tatsuoka, F. (2000): Stress history-dependent deformation characteristics of dense sand in plane strain, *Soils and Foundations*, **40**(2), 55–74.